A Digital Technique for Art Authentication

Siwei Lyu[1], Daniel Rockmore[1,2], and Hany Farid[1,†]
Department of Computer Science[1] and Mathematics[2]
Dartmouth College
Hanover NH 03755

We describe a computational technique for authenticating works of art, specifically, paintings and drawings, from high resolution digital scans of the original works. This approach builds a statistical model of an artist from the scans of a set of authenticated works, against which new works are then compared. The statistical model consists of first- and higher-order wavelet statistics. We show preliminary results from our analysis of thirteen drawings that have at various times been attributed to Pieter Bruegel the Elder, which confirm expert authentications. We also apply these techniques to the problem of determining the number of artists that may have contributed to a painting attributed to Perugino and again achieve an analysis agreeing with expert opinion.

1 Introduction

It probably wasn't long after people began paying money for art that a lucrative business in forging art was born. And it probably wasn't too much later that techniques for detecting art forgeries emerged. Even today, the early techniques for authentication remain pre-eminent. By and large these are based on "connoisseurship" and so rely upon the discerning eyes of a few experts who are steeped in the work and life of the artist in question. Their opinion may be informed by the *catalogue raisson* which is the current acknowledged authoritative work on the artist's œuvre. Other desiderata may include provenance which might be traced back to the artist's circle or his collectors and makes possible the comparison of the work's implicit biography with the histories of related works, or even a detailed analysis of any signature that may be present. (See [19] for a survey of current techniques.)

In addition to the reliance on the human actor, quantitative methods can be brought to bear. X-ray analysis can reveal a painting beneath a painting that can shed light on its origins. Surface analysis of the painting materials is another approach, most famously applied in the investigation of the famous "van Meerghen forgeries." In this case, the forgery of paintings attributed to Vermeer was confirmed by dating the paintings according to the proportion of a certain lead isotope in the lead-based paint. An elementary application of differential equations allows for the actual isotope content to be compared with the expected content had the work been painted in Vermeer's day [10]. This marks a first use of mathematics in the service of authentication.

With the advent of powerful digital technology, computational tools may be able to provide new insights and techniques into the art and science of art authentication. For example, a fractal analysis of Jackson Pollock's drip paintings has revealed interesting relations between the evolution of Pollock's aesthetic and the fractal dimension of his work [21, 20]. The analysis also raises the possibility of using fractal dimension to help authenticate Pollock. Various techniques from machine learning have been applied to the analysis and classification of *craquelure* – the crack lines that appear over time in a painting [2].

In this paper we present a new computational tool for analyzing prints, drawings and paintings for use in authentication. Specifically, we perform a multi-scale, multi-orientation image decomposition (e.g., wavelets) of a collection of high-resolution digital scans of a drawing or painting. This decomposition changes the basis from functions maximally localized in space (pixels) to one in which the basis functions are localized not only in space, but also in orientation and scale. A familiar analogy comes from sound, where the original sound might be transformed

† Correspondence should be addressed to H. Farid. 6211 Sudikoff Lab, Department of Computer Science, Dartmouth College, Hanover NH 03755. tel/fax: 603.646.2761/1672; email: farid@cs.dartmouth.edu.

into a vector of local frequency information which reflects how much of each frequency comprises the original sound over a short time window. We construct a compact model of the statistics from such a multi-scale, multi-orientation image decomposition, and look for consistencies or inconsistencies across different drawings or paintings, or within a single work. The latter is the so-called "problem of many hands" in which we try to determine the regions of a collaborative work that have been accomplished by a single artist.

The analysis produces local oriented spatial frequency data, and so suggests that the accompanying model captures the subtle pen and brush strokes characteristic of an artist. Although an imitation [1] may be perceptually similar to an original (i.e., very much in the "style of the master"), the subtle differences in stroke can reveal the presence of an imitation. In a sense this work is a natural successor to the mathematical techniques used for graphology, or handwriting analysis (see e.g., [11]), distilling not just the characteristic lines and curves of a painter's literal signature, (which is often part of the process of authentication) but even more, moving toward a characterization of the artist's aesthetic signature, resident within the line and curve of his or her work.

Analogous techniques have already made their way into the literary world, where they fall within the discipline of *stylometry* [8]. The problem of classification has been applied to divvying up the attribution of the Federalist papers between Madison and Hamilton (see e.g., [13]) and the determination of the authorship of the fifteenth book in the Oz series [3]. Statistical approaches to the question of authentication have surfaced in the analysis of Shakespeare's sonnets [22]. The problem of many hands finds its mirror in a study of the conjectured multiple authorship of the Old Testament [7].

We begin by applying our analysis to the problem of authentication of a collection of thirteen drawings

[1] Henceforth we will give the benefit of the doubt to the imitator and use the terminology "imitation" rather than the more charged "forgery."

MMA Cat. No.	Title	Artist
3	Pastoral Landscape	Bruegel
4	Mountain Landscape with Ridge and Valley	Bruegel
5	Path through a Village	Bruegel
6	Mule Caravan on Hillside	Bruegel
9	Mountain Landscape with Ridge and Travelers	Bruegel
11	Landscape with Saint Jermove	Bruegel
13	Italian Landscape	Bruegel
20	Rest on the Flight into Egypt	Bruegel
7	Mule Caravan on Hillside	-
120	Mountain Landscape with a River, Village, and Castle	-
121	Alpine Landscape	-
125	Solicitudo Rustica	-
127	Rocky Landscape with Castle and a River	Savery

Figure 1: Authentic (top) and imitations (bottom). The first column corresponds to the Metropolitan Museum of Art (MMA) catalog number in [14].

that have at one time or another been attributed to the famous draughtsman Pieter Bruegel the Elder. We then follow with a "many-hands" analysis of a portrait by the great Renaissance painter Perugino. We close with a synopsis of the tools used in the analysis and describe the underlying statistical model. We collect some of the more technical points in an appendix.

2 Bruegel

The Flemish painter and draftsman, Pieter Bruegel the Elder (1525/30-1569) was among the greatest artists of the sixteenth century. Of particular beauty and fame are Bruegel's landscape drawings. Over time he acquired many imitators, some undoubtedly simply eager to work in the style of the great master,

while others surely hoping to pass off their work as Bruegel's for monetary gain. Some of these followers and imitators were expert enough that after being unmasked (or discovered) they became famous in their own right e.g., Jacob Savery. Bruegel's work has recently been the subject of renewed study and interest [12, 14, 15]. As a result many drawings formerly attributed to Bruegel are now attributed to others.

The delicate line and shading comprising these works suggests that their classification according to a wavelet-like analysis may be both appropriate and fruitful. For our analysis we digitally scanned (at 2400 dpi) eight authenticated drawings by Bruegel and five acknowledged Bruegel imitations from 35mm color slides, Figure 1 (slides were provided courtesy of the Metropolitan Museum of Art [14]). These color (RGB) images, originally of size 3894×2592, were cropped to a central 2048×2048 pixel region, converted to grayscale [2] (gray = 0.299R + 0.587G + 0.114B), and autoscaled to fill the full intensity range $[0, 255]$. Shown in Figure 2 are examples of an authentic drawing and an imitation.

Each digital image was then subdivided into 64 non-overlapping 256×256 pixel regions. Each of these subimages was then transformed using a five-level, three-orientation wavelet-like decomposition (see Section 4 for details). From this decomposition, a 72-length feature vector of coefficient and error statistics is extracted for each subimage (Section 4.) Each drawing now corresponds to a set of points in this 72-D space. Authentication is indicated by the distance between these point clouds, with the belief that works by the same artist will be close together, irrespective of content, and an imitation will be relatively far from the authenticated Bruegels. Thus, we first computed the Hausdorff distance [9] between all pairs of images (Appendix A). The resulting 13×13 distance ma-

[2] While converting from color to grayscale results in a significant loss of information, we did so in order to make it more likely that the measured statistical features and subsequent classification was more likely to be based on the artist's strokes, and not on simple color differences.

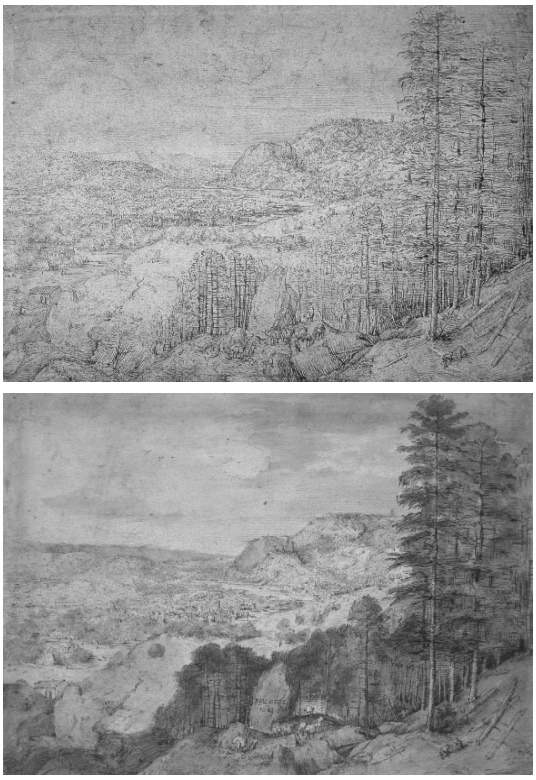

Figure 2: Authentic #6 (top) and imitation #7 (bottom), see Table 1.

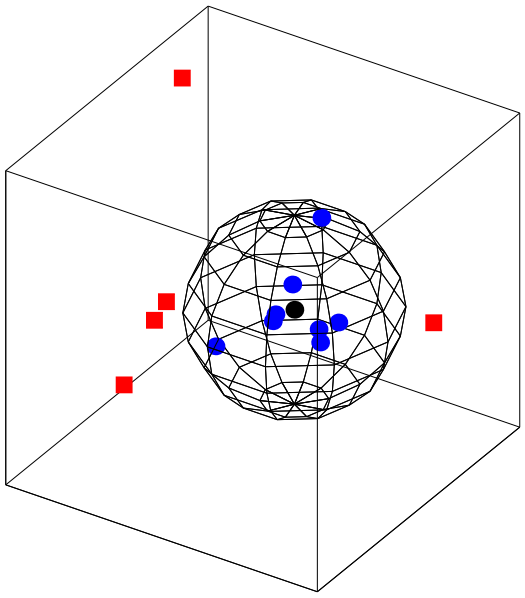

Figure 3: Results of analyzing 8 authentic Bruegel drawings (blue circles) and 5 imitations (red squares). Note how the imitations lie significantly outside of the bounding sphere of authentic drawings.

trix was then subjected to a multidimensional scaling (MDS) [5] (Appendix B). Shown in Figure 3 is the result of visualizing the original 13 images in a lower-dimensional space as determined by a MDS analysis. The blue circles in Figure 3 correspond to the authentic drawings, and the red squares to the imitations. For purposes of visualization the wire-frame sphere is rendered at the center of mass of the eight authenticated drawings and with a radius set to fully encompass all eight data points (in so doing, we assume knowledge of the authenticated Bruegels). Note that all five imitations fall well outside of the sphere. The distances from the authenticated Bruegels to the center of the sphere are 0.34, 0.35, 0.55, 0.90, 0.56, 0.17, 0.54, and 0.85. The distances from the imitations are considerably larger at 1.58, 2.20, 1.90, 1.48, and 1.33 (the means of these two distance populations are statistically significant: $p < 1^{-5}$ (one-way anova)). Even in this space of reduced dimension, there is a clear difference between the authentic drawings and the imitations.

3 Perugino

Pietro di Cristoforo Vannucci (Perugino) (1446-1523) is well known as a portraitist and a fresco painter, but perhaps he is best known for his altarpieces. By the 1490s Perugino maintained a workshop in Florence as well as in Perugia and was quite prolific. Shown in Figure 4 is the painting Madonna With Child by Perugino. As with many of the great Renaissance paintings, however, it is likely that Perugino only painted a portion this work - apprentices did the rest. To this end, we wondered if we could uncover statistical differences amongst the faces of the individual characters.

The painting (at the Hood Museum, Dartmouth College) was photographed using a large-format camera (8×10 inch negative) and drum-scanned to yield a color $16,852 \times 18,204$ pixel image. As in the previous section this image was converted to grayscale. The

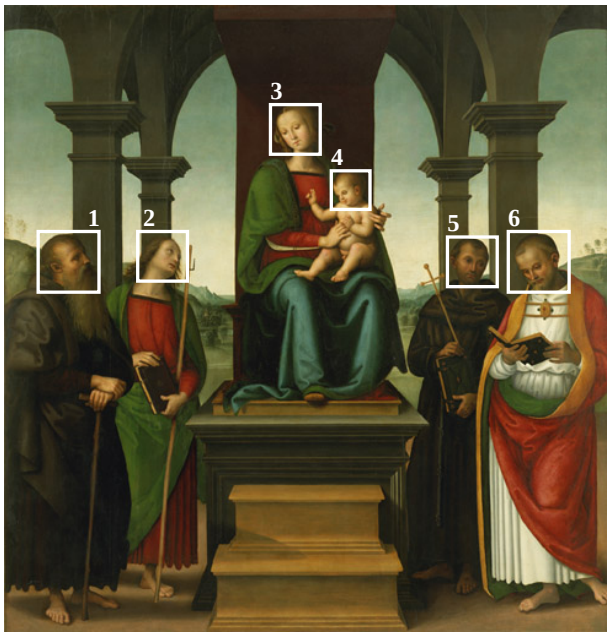

Figure 4: Madonna With Child by Perugino. How many hands contributed to this painting?

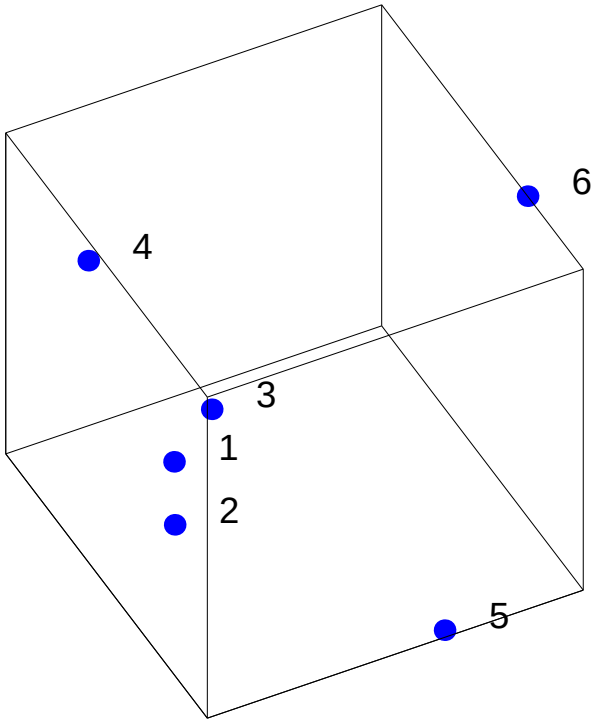

Figure 5: Results of analyzing the Perugino painting. The numbered data points correspond to the six faces (from left to right) in Figure 4. Note how the three left-most faces (1-3) cluster, while the remaining faces are distinct. This clustering pattern suggests the presence of at least four distinct hands.

facial region of each of the six characters was manually localized. Each face was then partitioned into non-overlapping 256×256 regions and auto-scaled into the full intensity range $[0, 255]$. This partitioning yielded (from left to right) 189, 171, 189, 54, 81, and 144 regions. The same set of statistics as described in the previous section was collected from each of these regions. Also as in the previous section, we computed the Hausdorff distance (Appendix A) between all pairs of six faces. The resulting 6×6 distance matrix was then subjected to MDS (Appendix B). Shown in Figure 5 is the result of visualizing the original six faces in a lower-dimensional space as determined by a MDS analysis.

The numbered data points correspond to the six faces (from left to right) in Figure 4. Note how the three left-most faces cluster, while the remaining faces are distinct. The average distance between faces $1 - 3$ is 0.61, while the average distance between the other faces is 1.79. This clustering pattern suggests the presence of at least four distinct hands, and is consistent with the views of some art historians [1].

4 Methods

Our methodology makes use of a decomposition of images using basis functions that are localized in spatial position, orientation, and scale (e.g., wavelets). These sorts of expansions have proven extremely useful in a range of applications (e.g., image compression, image coding, noise removal, and texture synthesis). One reason for this is that such decompositions exhibit statistical regularities that can be exploited (e.g., [17, 16, 4]). Described below is one such decomposition, and a set of statistics collected from this decomposition. [3]

[3] We also have experimented with both Laplacian and steerable pyramid decompositions. Results from a steerable pyramid (with eight orientation subbands) were similar to the results included above (which use only three orientation subbands). Furthermore, the Laplacian pyramid generally gave poor results. So while it seems that oriented subbands are necessary, it also seems that a finer tuning of orientation is not necessary for this particular task.

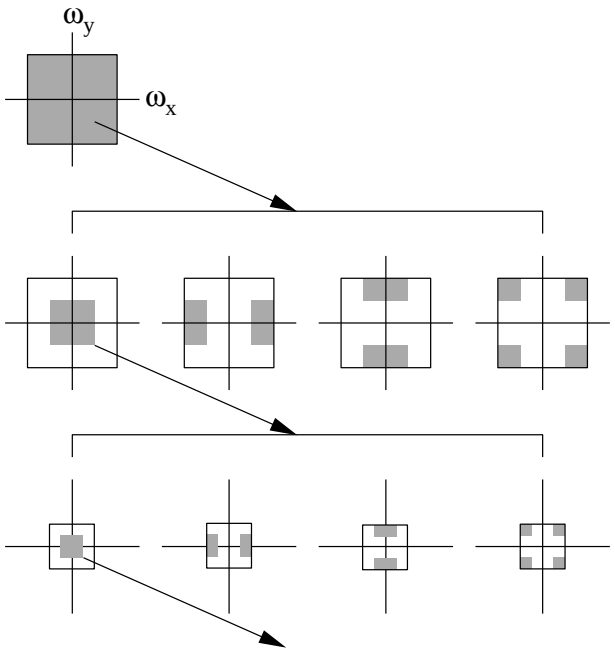

Figure 6: An idealized multi-scale and orientation decomposition of frequency space. Shown, from top to bottom, are levels 0,1, and 2, and from left to right, are the lowpass, vertical, horizontal, and diagonal subbands.

The decomposition is based on separable quadrature mirror filters (QMFs) [23, 24, 18]. As illustrated in Figure 6, this decomposition splits the frequency space into multiple scales and orientations. This is accomplished by applying separable lowpass and highpass filters along the image axes generating a vertical, horizontal, diagonal and lowpass subband. For example, the horizontal subband is generated by convolving with the highpass filter in the horizontal direction and lowpass in the vertical direction, the diagonal band is generated by convolving with the highpass filter in both directions, etc. Subsequent scales are created by subsampling the lowpass by a factor of two and recursively filtering. The vertical, horizontal, and diagonal subbands at scale $i = 1, ..., n$ are denoted as $V_i(x, y)$, $H_i(x, y)$, and $D_i(x, y)$, respectively. Shown in Figure 7 is a three-level decomposition of

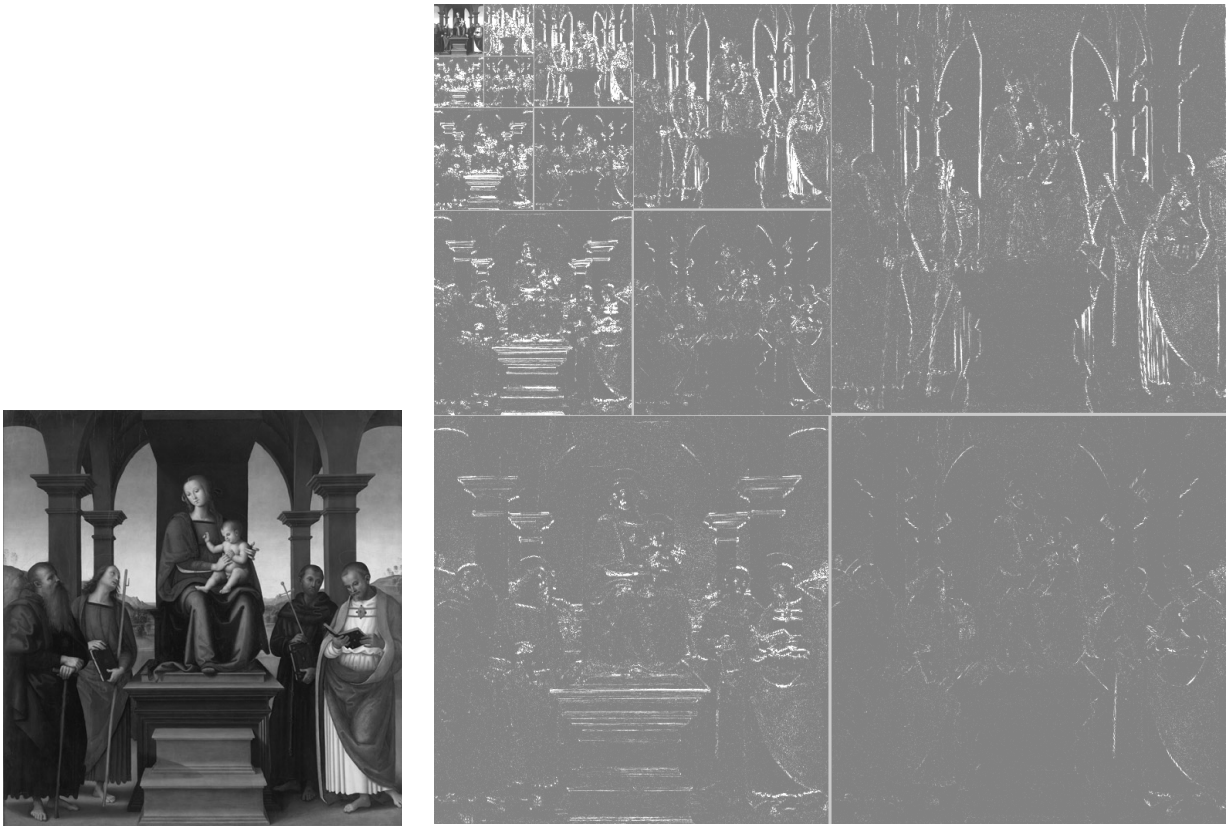

Figure 7: Shown on the right are the absolute values of the subband coefficients at three scales and three orientations (the residual lowpass subband is shown in the upper-left corner) for the Perugino (left).

the scanned Perugino, shown in the same figure.

Given this image decomposition, the statistical model is composed of the mean, variance, skewness and kurtosis of the subband coefficients at each orientation and at scales $i = 1, ..., n-2$. These statistics characterize the basic coefficient distributions. In order to capture the higher-order correlations that exist within this image decomposition, these coefficient statistics are augmented with a set of statistics based on the errors in an optimal linear predictor of coefficient magnitude.

As described in [4], the subband coefficients are correlated to their spatial, orientation and scale neighbors. For purposes of illustration, consider first a vertical band, $V_i(x, y)$, at scale i. A linear predictor for the magnitude of these coefficients in a subset of all possible neighbors may be given by:

$$\begin{aligned} |V_i(x,y)| &= w_1|V_i(x-1,y)| + w_2|V_i(x+1,y)| \\ &+ w_3|V_i(x,y-1)| + w_4|V_i(x,y+1)| \\ &+ w_5|V_{i+1}(\tfrac{x}{2},\tfrac{y}{2})| + w_6|D_i(x,y)| \\ &+ w_7|D_{i+1}(\tfrac{x}{2},\tfrac{y}{2})|, \end{aligned} \quad (1)$$

where w_k denotes scalar weighting values, and $|\cdot|$ denotes magnitude. This particular choice of spatial, orientation, and scale neighbors was employed in our earlier work on detecting traces of digital tampering in images [6]. Here we employ an iterative brute-force search (on a per subband and per image basis) for the set of neighbors that minimizes the prediction error within each subband.

Consider again the vertical band, $V_i(x, y)$, at scale i. We constrain the search of neighbors to a 3×3 spatial

region at each orientation subband and at three scales, namely, the neighbors:

$$
\begin{aligned}
&V_i(x-c_x, y-c_y), H_i(x-c_x, y-c_y),\\
&D_i(x-c_x, y-c_y),\\
&V_{i+1}(\tfrac{x}{2}-c_x, \tfrac{y}{2}-c_y), H_{i+1}(\tfrac{x}{2}-c_x, \tfrac{y}{2}-c_y),\\
&D_{i+1}(\tfrac{x}{2}-c_x, \tfrac{y}{2}-c_y),\\
&V_{i+2}(\tfrac{x}{4}-c_x, \tfrac{y}{4}-c_y), H_{i+2}(\tfrac{x}{4}-c_x, \tfrac{y}{4}-c_y),\\
&D_{i+2}(\tfrac{x}{4}-c_x, \tfrac{y}{4}-c_y),
\end{aligned}
$$

with $c_x = \{-1, 0, 1\}$ and $c_y = \{-1, 0, 1\}$, and, of course, excluding $V_i(x, y)$. From these 80 possible neighbors, the iterative search begins by finding the single most predictive neighbor (e.g., $V_{i+1}(x/2-1, y/2)$) [4]. This neighbor is held fixed and the next most predictive neighbor is found. This process is repeated five more times to find the optimally predictive neighborhood. On the k^{th} iteration, the predictor coefficients $(w_1, ..., w_k)$ are determined as follows. Let the vector $\vec{V}$ contain the coefficient magnitudes of $V_i(x, y)$ strung out into a column vector, and the columns of the matrix Q contain the chosen neighboring coefficient magnitudes also strung out into column vectors. The linear predictor then takes the form:

$$\vec{V} \quad = \quad Q\vec{w}, \tag{2}$$

where the column vector $\vec{w} = (\, w_1 \quad \dots \quad w_k \,)^T$, The predictor coefficients are determined by minimizing the quadratic error function:

$$E(\vec{w}) \quad = \quad [\vec{V} - Q\vec{w}]^2. \tag{3}$$

This error function is minimized by differentiating with respect to $\vec{w}$:

$$dE(\vec{w})/d\vec{w} \quad = \quad 2Q^T[\vec{V} - Q\vec{w}], \tag{4}$$

setting the result equal to zero, and solving for $\vec{w}$ to yield:

$$\vec{w} \quad = \quad (Q^TQ)^{-1}Q^T\vec{V}. \tag{5}$$

[4] Integer rounding is used when computing the spatial positions of a parent, e.g., $x/2$ or $x/4$.

The log error in the linear predictor is then given by:

$$\vec{E_v} \quad = \quad \log_2(\vec{V}) - \log_2(|Q\vec{w}|). \tag{6}$$

Once the full set of neighbors is determined additional statistics are collected from the errors of the final predictor - namely the mean, variance, skewness, and kurtosis. This entire process is repeated for each oriented subband, and at each scale $i = 1, ..., n-2$, where at each subband a new set of neighbors is chosen and a new linear predictor estimated.

For a n-level pyramid decomposition, the coefficient statistics consist of $12(n-2)$ values, and the error statistics consist of another $12(n-2)$ values, for a total of $24(n-2)$ statistics. These values represent the measured statistics of an artist's style and are used to classify or cluster drawings or paintings.

As stated above, following the computation of the feature vectors multi-dimensional scaling (MDS) was employed to project the original 72-D feature vectors into a 3-D subspace. Features with no discriminating power (e.g., the means) will therefore play no role in the lower-dimensional embedding.

5 Discussion

We have presented a computational tool for digitally authenticating or classifying works of art. This technique looks for consistencies or inconsistencies in the first- and higher-order wavelet statistics collected from drawings or paintings (or portions thereof). We showed preliminary results from our analysis of thirteen drawings either by, or in the style of, Pieter Bruegel the Elder as well as a painting by Perugino. We expect these techniques, in collaboration with existing physical authentication, to play an important role in the field of art forensics.

References

[1] Personal correspondence with Timothy B. Thurber, Hood Museum, Dartmouth College.

[2] F. S. Abas and K. Martinez. Classification of painting cracks for content-based retrieval. In *IS&T/SPIE's 15th Annual Symposium on Electronic Imaging: Machine Vision Applications in Industrial Inspection XI*, Santa Clara, CA, 2003.

[3] J.N.G. Binong. An application of multivariate analysis to authorship attribution. *Chance*, 16(2):9–17, 2003.

[4] R.W. Buccigrossi and E.P. Simoncelli. Image compression via joint statistical characterization in the wavelet domain. *IEEE Transactions on Image Processing*, 8(12):1688–1701, 1999.

[5] T. Cox and M. Cox. *Multidimensional Scaling*. Chapman & Hall, London, 1994.

[6] H. Farid and S. Lyu. Higher-order wavelet statistics and their application to digital forensics. In *IEEE Workshop on Statistical Analysis in Computer Vision (in conjunction with CVPR)*, Madison, WI, 2003.

[7] R. Friedman. *Who Wrote the Bible?* Harper, San Francisco, CA, 1997.

[8] D. I. Holmes and J. Kardos. Who was the author? an introduction to stylometry. *Chance*, 16(2):5–8, 2003.

[9] D.P. Huttenlocher, G.A. Klanderman, and W.J. Rucklidege. Comparing images using the hausdorff distance. *IEEE Transactions on Pattern Analysis and Machine Intelligence*, 15(9):850–863, 1993.

[10] B. Keisch. Dating works of art through their natural radioactivity: improvements and applications. *Science*, 160:413–415, 1968.

[11] I.W. McKeague. A statistical model for signatures. *Journal of the Amercican Statistical Association*, page (in press), 2004.

[12] U. Mielke, editor. *Pieter Bruegel, Die Zeichnungen*. Brepols, Turnhout, Belgium, 1996.

[13] F. Mosteller and D. L. Wallace. *Applied Bayesian and Classical Inference: The Case of the Federalist Paper*. Springer-Verlag, New York, NY, 1984.

[14] N.M. Orenstein, editor. *Pieter Bruegel the Elder*. Yale University Press, New Haven and London, 2001.

[15] N.M. Orenstein. Followers and fakers of pieter bruegel. *International Foundation for Art Research Journal*, 6(3):12–17, 2003.

[16] R. Rinaldo and G. Calvagno. Image coding by block prediction of multiresolution submimages. *IEEE Transactions on Image Processing*, 4(7):909–920, 1995.

[17] J. Shapiro. Embedded image coding using zerotrees of wavelet coefficients. *IEEE Transactions on Signal Processing*, 41(12):3445–3462, 1993.

[18] E.P. Simoncelli and E.H. Adelson. *Subband image coding*, chapter Subband transforms, pages 143–192. Kluwer Academic Publishers, Norwell, MA, 1990.

[19] R.D. Spencer, editor. *The Expert Versus the Object*. Oxford University Press, 2004.

[20] R. Taylor. Pollock, Mondrian and the nature: Recent scientific investigations. *Chaos and Complexity Letters*, in press.

[21] R. Taylor, A.P. Micolich, and D. Jones. Fractal analysis of Pollock's drip paintings. *Nature*, 399:422, 1999.

[22] R. Thisted and B. Efron. Did shakespeare write a newly-discovered poem? *Biometrika*, 74:445–455, 1987.

[23] P.P. Vaidyanathan. Quadrature mirror filter banks, M-band extensions and perfect reconstruction techniques. *IEEE ASSP Magazine*, pages 4–20, 1987.

[24] M. Vetterli. A theory of multirate filter banks. *IEEE Transactions on ASSP*, 35(3):356–372, 1987.

Acknowledgments

D. Rockmore has been supported by grant AFOSR F49620-00-1-0280. H. Farid has been supported by an Alfred P. Sloan Fellowship, an NSF CAREER Grant (IIS-99-83806), a Department of Justice Grant (2000-DT-CS-K001), and a departmental NSF Infrastructure Grant (EIA-98-02068). We are grateful to George Goldner and Nadine Orenstein of New York City's Metropolitan Museum of Art and Kathy Hart of Dartmouth's Hood Museum of Art for their assistance and cooperation.

Appendix A: Hausdorff Distance

The Hausdorff distance is a distance metric defined on two sets of vectors, X and Y. The metric, $H(\cdot,\cdot)$ is defined as:

$$H(X,Y) = \max\left(h(X,Y), h(Y,X)\right),$$

where $h(\cdot,\cdot)$ is defined as:

$$h(X,Y) = \max_{\vec{x}\in X}\left(\min_{\vec{y}\in Y} d(\vec{x},\vec{y})\right).$$

Here $d(\cdot,\cdot)$ can be any distance metric defined on the vector space subsuming X and Y. In our case, we use Euclidean distance $d(\vec{x},\vec{y}) = (\vec{x}-\vec{y})^T(\vec{x}-\vec{y})$.

Appendix B: Multidimensional Scaling

Multidimensional scaling (MDS) is a popular method to visualize high dimensional data. Given n vectors $\{\vec{x}_1,\cdots,\vec{x}_n\}$, where $\vec{x}_i \in \mathcal{R}^m$, the goal of MDS is to find a lower-dimensional embedding for these data that minimally distorts their pairwise distances. Denote the $n\times n$ distance matrix as $D_{ij} = d(\vec{x}_i,\vec{x}_j)$, where $d(\cdot,\cdot)$ is a distance metric in $\mathcal{R}^m$. The most common such metric is Euclidean distance defined as $d(\vec{x}_i,\vec{x}_j) = (\vec{x}_i-\vec{x}_j)^T(\vec{x}_i-\vec{x}_j)$.

Given the pairwise symmetric distance matrix, the classic (metric) MDS algorithm is given by the following steps:

1. Let $A_{ij} = -\frac{1}{2}D_{ij}^2$.
2. Let $B = HAH$, where $H = I_n - \frac{1}{n}\vec{u}\vec{u}^T$, I_n is a $n\times n$ identity matrix, and each component of the n-dimensional vector $\vec{u}$ is 1.
3. Compute the eigenvectors, $\vec{e}_1,\cdots,\vec{e}_n$, and corresponding eigenvalues, $\lambda_1,\cdots,\lambda_n$, of matrix B, where $\lambda_1 \geq \lambda_2 \geq \cdots \geq \lambda_n$.
4. The new, lower-dimensional, representation of the original data, $\vec{x}_i$, are then given by $\vec{x'}_i = (\,\vec{e}_1(i) \quad \vec{e}_2(i) \quad \cdots \quad \vec{e}_{m'}(i)\,)$, where $\vec{e}_k(i)$ denotes the i^{th} component of the vector, and in our examples $m' = 3$.